Journal of Colloid and Interface Science xxx (2014) xxx–xxx

Contents lists available at ScienceDirect

Journal of Colloid and Interface Science

www.elsevier.com/locate/jcis

In vitro evaluation of graphene oxide nanosheets on immune function

M.J. Feito [a], M. Vila [b,c,d], M.C. Matesanz [a], J. Linares [a], G. Gonçalves [d], P.A.A.P. Marques [d], M. Vallet-Regí [b,c], J.M. Rojo [e], M.T. Portolés [a,*]

[a] Department of Biochemistry and Molecular Biology I, Faculty of Chemistry, Universidad Complutense, 28040 Madrid, Spain
[b] Department of Inorganic and Bioinorganic Chemistry, Faculty of Pharmacy, UCM, Instituto de Investigación Sanitaria Hospital 12 de Octubre i+12, 28040 Madrid, Spain
[c] Networking Research Center on Bioengineering, Biomaterials and Nanomedicine, CIBER-BBN, Spain
[d] TEMA-NRD, Mechanical Engineering Department and Aveiro Institute of Nanotechnology (AIN), University of Aveiro, 3810-193 Aveiro, Portugal
[e] Department of Cellular and Molecular Medicine, Centro de Investigaciones Biológicas, CSIC, 28040 Madrid, Spain

ARTICLE INFO

Article history:
Received 9 May 2014
Accepted 4 July 2014
Available online xxxx

Keywords:
Biocompatibility
Cytokine
Grapheme oxide
Lymphocyte
Macrophage

ABSTRACT

Hypothesis: Graphene oxide (GO) has attracted the scientific community attention due to its novel properties and wide range of potential applications including hyperthermia cancer therapy. However, little is known about the GO effects on the immune function which involves both innate and adaptive defence mechanisms through the activation of different cell populations and secretion of several cytokines. The effect of different GO nanosheets designed for hyperthermia cancer therapy on macrophage and lymphocyte function should be determined before using GO for this application.
Experiments: The effects of GO nanosheets with 1 (1-GOs) and 6 arms (6-GOs) of polyethylene glycol on RAW-264.7 macrophages and primary splenocytes (as approximation to the *in vivo* situation) were evaluated through the proinflammatory cytokine secretion and the modulation of cell proliferation in the presence of specific stimuli for either T-lymphocytes (concanavalin A, anti-CD3 antibody) or B-lymphocytes/macrophages (lipopolysaccharide).
Findings: 6-GOs significantly increased the secretion of TNF-α by RAW-264.7 macrophages without alteration of IL-6 and IL-1β levels. The treatment of primary splenocytes with 1-GOs and 6-GOs in the presence of concanavalin A, anti-CD3 antibody and lipopolysaccharide, produced significant dose-dependent decreases of cell proliferation and IL-6 levels, revealing weak inflammatory properties of GOs which are favourable for hyperthermia cancer therapy.

1. Introduction

Graphene has attracted the attention of the scientific community due to its novel properties and wide range of potential applications in electronics and energy conversion [1], drug delivery [2,3], tissue engineering [4,5], hyperthermia cancer therapy [6–8], gene delivery [9,10] and imaging [2]. Actually, GO can be simply defined as a plane of carbon atoms in aromatic structure with carboxylic and carbonyl groups on the edges and hydroxyl and epoxy groups in basal planes [11]. In fact, the high density and diversity of oxygen functional groups on GO surface provides reactive sites for chemical functionalization allowing the development of new multifunctional materials [12]. In this sense, the functionalization of the nanoparticles with biocompatible polymers such as polyethylene glycol (PEG) increases their stability in physiological conditions, minimizing the interactions with other biomolecules and reducing the risk of immunological response [13,14].

The biocompatibility of GO has begun to be investigated in different experimental models [15] showing lower *in vitro* toxicity than carbon nanotubes [16]. *In vivo* tests in mice show that GO exhibits dose-dependent toxicity after intravenous administration and it is mainly located in lung, liver and spleen, causing some alterations in these tissues [16,17]. Little is known about the effects of GO on the immune system. However, the evaluation of a biomaterial effects on immune cells is an essential component of its biocompatibility assessment [18–20]. The immune response comprises both innate and adaptive defence mechanisms which coordinately activate different cell populations and the secretion of several molecules with the purpose of eliminating foreign

* Corresponding author. Address: Departamento de Bioquímica y Biología Molecular I, Facultad de Ciencias Químicas, Universidad Complutense, 28040 Madrid, Spain. Fax: +34 1 394 41 59.
E-mail addresses: mjfeito@pdi.ucm.es (M.J. Feito), mvila@farm.ucm.es (M. Vila), conchitamatesanz@hotmail.com (M.C. Matesanz), javilinares_88@hotmail.com (J. Linares), ggoncalves@ua.pt (G. Gonçalves), paulam@ua.pt (P.A.A.P. Marques), vallet@farm.ucm.es (M. Vallet-Regí), jmrojo@cib.csic.es (J.M. Rojo), portoles@quim.ucm.es (M.T. Portolés).

http://dx.doi.org/10.1016/j.jcis.2014.07.004
0021-9797/

agents. The innate immune response includes recruiting of macrophages and monocytes to sites of infection or biomaterial implantation, through the production of chemical mediators (cytokines), activation of the complement cascade, and phagocytosis. The activated cells promote antigen recognition, clearance of dead cells or antibody complexes and respond producing reactive oxygen and nitrogen species, antimicrobial peptides, and inflammatory mediators [21,22]. On the other hand, the adaptive immune response is mediated by antigen-specific lymphocytes (T and B cells) and by their products, which include inflammatory cytokines and antibodies. In this sense, the initial response to biomaterials includes the secretion of inflammatory cytokines and growth factors by macrophages and lymphocytes. The cytokines IL-1β, IL-6, TNF-α are regarded as typical proinflammatory cytokines, whereas the chemokines IL-8, MCP-1, and MIP-1β (regulated upon activation, normal T-cell expressed, and secreted) are responsible for the recruitment of monocytes, all of them participate as mediators producing inflammation and wound healing [23]. Concerning macrophages, two functional phenotypes have been described, namely classically activated macrophages (M1) and alternatively activated macrophages (M2) [24–26]. M1 macrophages, induced by IFN-γ and/or TNF-α, show a Th1-like $CD4^{+}$T-cells phenotype, have proinflammatory effects, are involved in cellular immunity, and have bactericidal functions. On the other hand, M2 macrophages which include at least three different overlapping phenotypes, (M2 a, b, and c), are generated by different mediators, exhibit a Th2-like $CD4^{+}$T-cells phenotype primed by interleukin 4 (IL-4) and IL-13 (M2a subset), immune complexes and LPS (M2b subset), or IL-10 (M2c subset) and are involved in humoral immunity, resolution of inflammation, and tissue repair.

Besides their role as inflammatory mediators, macrophages also have the remarkable ability of presenting antigens to T cells, thereby initiating the mechanisms of adaptive immunity. T lymphocytes have been demonstrated to promote macrophage adhesion and fusion via paracrine effects [27]. T cell activation via antigen presentation does not occur with synthetic biomaterials as they are not degradable, however it has been suggested that synthetic biomaterials may present functional groups on their surfaces acting as mitogens [28]. Generally, T cell activation occurs after a series of events following appropriate stimulation. When specific peptides presented in the context of MHC engage with the antigen receptor of T cells (TCR) and with adequate co-stimulation, they activate signal transduction pathways involving mitogen-activated protein kinase (MAPK), phosphatidylinsositol-3 kinase (PI3K)-Akt and intracellular Ca^{+2}/protein kinase C in target cells. Eventually, T lymphocyte activation leads to changes in other parameters including up-regulation of activation markers and cytokine secretion.

Graphene and its derivatives interact with macrophages, and recent studies demonstrate the capability of phagocytes for internalizing graphene oxide [20]. On the other hand, Schinwald et al. have reported that graphene nanoplatelets cause inflammatory responses *in vivo* and *in vitro* [29].

In the present study, we investigated the *in vitro* action of graphene oxide nanosheets (GOs) with 1 (1-GOs) and 6 arms (6-GOs) of PEG on murine macrophages and lymphocytes in order to determine if the exposure to these materials, designed for hyperthermia cancer therapy, results in modulation of either innate or adaptive immunity. With this aim, the effects of 1-GOs and 6-GOs on RAW-264.7 macrophages and primary splenocytes (including macrophages, B and T lymphocytes) obtained from C57BL/6 mice, were evaluated through the production of proinflammatory cytokines and the modulation of immune cell proliferation in the presence of specific stimuli as concanavalin A and anti-CD3 antibody (for T-lymphocytes) or lipopolysaccharide (for B-lymphocytes and macrophages).

2. Material and methods

2.1. GO nanosheet preparation and characterization

GO nanosheets of c.a. 100 nm have been obtained from exfoliation of high purity graphite in acidic medium by a modified Hummers method [30]. Briefly, 2 g of graphite (99.99%; Sigma–Aldrich) was dispersed into a flask containing 50 ml of concentrated H_2SO_4 and 7 g of $KMnO_4$ and the solution was magnetically stirred for 2 h. Then, the solution was treated with H_2O_2 until the gas evolution ceased, and the resultant suspension was intensively washed, first with HCl solution (0.1 mol dm^{-3}) and then with distilled water by filtration and centrifugation. The resulting GO suspension was dialyzed until a pH of 7 was reached.

After 3 h of further ultrasonic treatment to reduce the lateral size (50–100 nm), 50 ml of graphite oxide in water (~1 mg/ml) were activated with 2.5 g of chloroacetic acid (Cl—CH_2—COOH) under strongly basic conditions (2.5 g NaOH) in order to promote —COOH groups at its surface, and bath sonicated for 3 h. The resulting GO solution was neutralized and purified by repeated rinsing and filtrations.

Transmission electron microscopy (TEM) was performed on a 200 kV JEOL JEM 2100. Dynamic light scattering (DLS) particle size analysis measurements were also performed in pH 5.5 solutions in a Zetasizer Nano Series instrument equipped with a 633 nm 'red' laser from Malvern Instruments, with reproducibility being verified by collection and comparison of sequential measurements. Micro-Raman experiments were performed at room temperature using the 488 nm line of an Ar+ laser with an incident power of 1 mW, and XPS using a VG Scientific ESCALAB 200 A; UK equipment.

2.2. Functionalization of GO with poly(ethylene glycol-amine) (PEG)

Activated GO was then functionalized by covalent bonding with non-toxic and non-immunogenic polymers poly(ethylene glycol-amine) (PEG) to avoid the aggregation. A diimide activation was performed by adding EDAC (1-ethyl-3-(3-dimethylaminopropyl) carbodiimide hydrochloride, Sigma Inc., 0.106 g) to 45 ml of GO aqueous solution (1 mg/ml) and stirred vigorously for 3 h. Afterwards this solution is added to a 25 ml solution of polyethylene glycol-amine (11 mg/ml) and the reaction was allowed to proceed for 48 h. Excess PEG was removed by centrifuge filtration. GO water suspensions were systematically washed by centrifugation through MWCO Amicon filters with 100 kDa molecular weight cut-off. Different branched PEG polymer were attached following the same route, 1-arm PEG bis(3-aminopropyl) terminated 1.5 kDa (Sigma) and 6-arm branched PEG amine 1.5 kDa (SunBio Inc.), samples named 1-GOs and 6-GOs respectively in order to study the influence of surface charge and polymer size on the uptake process.

2.3. GO nanosheet labeling with FITC

All GOs were marked with fluorescein isothiocyanate (FITC) covalent bonded to the PEG in order to control and follow GOs fate in the *in vitro* cell internalization studies. Pegylated GOs were redispersed in a pH 7.5 phosphate buffer (0.02 M) (0.5 mg/ml) and reacted with the amine reactive dye FITC. The reaction was allowed to proceed overnight at room temperature in the dark. Excess dye molecules were removed by centrifugation filtration through 100 kDa MWCO Amicon filters and washed away with water for over 10 times until no noticeable color in the filtrate. Afterwards, pegylated and fluorescein labeled GOs were liofilized.

2.4. Culture and treatment of RAW-264.7 macrophages for evaluation of FITC-GO nanosheet incorporation by flow cytometry

Murine RAW-264.7 macrophages were seeded on 6 well culture plates (CULTEK S.L.U., Madrid, Spain), at a density of 10^5 cells/ml in DMEM supplemented with 10% fetal bovine serum (FBS, Gibco, BRL), 1 mM L-glutamine (BioWhittaker Europe, Belgium), penicillin (200 μg/ml, BioWhittaker Europe, Belgium), and streptomycin (200 μg/ml, BioWhittaker Europe, Belgium), under a CO_2 (5%) atmosphere and at 37 °C for 24 h. To evaluate GO nanosheet incorporation by cultured RAW-264.7 cells, FITC-GO material (75 μg/ml) was added to the culture medium for 1 day. After treatment, cells were harvested using cell scrapers designed for harvesting cells and the incorporation of FITC-GO was evaluated by flow cytometry. The fluorescence of FITC was excited by a 15 mW laser tunning to 488 nm and the emitted fluorescence was measured with a 530/30 band pass filter in a FACScalibur Becton Dickinson flow cytometer.

Cell viability was determined by addition of propidium iodide (PI; 0.005% in PBS, Sigma–Aldrich Corporation, St. Louis, MO, USA) to stain the DNA of dead cells. The fluorescence of PI was excited by a 15 mW laser tuned to 488 nm and the emitted fluorescence was measured with a 670 nm long pass filter in a FACScalibur Becton Dickinson flow cytometer. Controls without material were always carried out.

2.5. Confocal microscopy studies

Murine RAW-264.7 macrophages were seeded on glass coverslips and cultured in the presence of FITC-GO materials for 24 h, fixed with 3.7% paraformaldehyde in PBS, permeabilizated with 0.1% Triton X-100 and preincubated with PBS containing 1% BSA. Then, cells were incubated for 20 min with rhodamine-phalloidin (1:40), stained with 4′-6-diamidino-2′-phenylindole (DAPI, 3 μM in PBS) and examined using a Leica SP2 Confocal Laser Scanning Microscope. Rhodamine fluorescence was excited at 540 nm and measured at 565 nm. DAPI fluorescence was excited at 405 nm and measured at 420–480 nm. FITC fluorescence was excited at 488 nm and measured at 491–586 nm.

2.6. Animal species selection and husbandry

Female C57BL/6 mice between 9 and 12 weeks of age were used in these studies. Mice were maintained on CIB, and they were housed in an isolated vivarium at optimal condition of temperature (21–24 °C) and humidity (40–70%). All procedures were approved by Institutional Animal Care and Use Committees.

2.6.1. Spleen cell suspension preparation

Splenocytes were obtained from spleen cell suspensions of C57BL/6 mice. The number of animals utilized in each study varied from 2 to 3 mice depending of the total number of cell required for each assay. After removal of erythrocytes by hypotonic shock they were gently washed with culture medium and resuspended in DMEM supplemented with 10% fetal bovine serum, 1 mM L-glutamine, penicillin (200 μg/ml), and streptomycin (200 μg/ml) before adjusting cell concentration.

2.7. Lymphocyte proliferation assays

Lymphocyte proliferation was performed as previously described with minor modifications. Briefly, splenocytes (2 × 106/ml; 50 μl/well) were cultured with or without GO nanosheet (75 μg/ml) at six different concentrations (100, 50, 25, 12.5, 6.25, 3.125 μl) in 96-well plates. Specifically, proliferation of T cells was evaluated following the stimulation with either the T-cell mitogen concanavalin A (Con A) (Amersham Pharmacia, Bjorkgatan, Sweden) (2.5 μg/ml final concentration, 50 μl/well) or anti-CD3 antibody (YCD3-1 rat IgG2b anti-mouse CD3) (5 μg/ml final concentration, 50 μl/well), whereas proliferation of B-cells was evaluated following the stimulation with lipopolysaccharide (LPS, *Escherichia coli* 055:B5) (100 μg/ml final concentration, 50 μl/well) [31]. Cultures were maintained at 37 °C, 5% CO_2 and 95% humidity. After 3 days, cell proliferation was determined by a colorimetric assay using 3-(4,5-dimethylthiazole-2-yl)-2,5 diphenyltetrazolium bromide (MTT) as described (Mossmann, 1983) [32]. The optical density (OD) of the formazan solution was read on a spectrophotometric plate reader (Labsystems Multiskan BIchromatic) at a wavelength of 570 nm.

2.8. Inflammatory cytokine detection

RAW-264.7 cells were incubated overnight either in the absence or in the presence of 1 μg/ml LPS (*E. coli* 055:B5) and then with GO materials during 1 day. Splenocytes plated at a density of 2×10^6/ml were seeded onto 96-well plates and incubated for 72 h as described above. The amounts of IL-1β, TNF-α, and IL-6 in the supernatants were quantified by ELISA (Gen-Probe, Diaclone), carried out according to the manufacturer's instructions.

2.9. Statistics

Data are expressed as means ± standard deviations of a representative of three experiments carried out in triplicate. Statistical analysis was performed using the Statistical Package for the Social Sciences (SPSS) version 19 software. Statistical comparisons were made by analysis of variance (ANOVA). Scheffé test was used for post hoc evaluations of differences among groups. In all of the statistical evaluations, $p < 0.05$ was considered as statistically significant.

3. Results and discussion

The evaluation of the biological responses to graphene oxide (GO) is a necessary step before using this attractive material for biomedical applications. Particularly, the immune response, involving macrophages and lymphocytes, may play a key role in the reaction of whole organisms to GO exposure. In the present study, GO nanosheets of ca 100 nm with 1 (1-GOs) and ca 300 nm with 6 arms (6-GOs) of polyethylene glycol, designed for hyperthermia cancer therapy, have been incubated with murine RAW-264.7 macrophages and primary splenocytes as experimental cell models. The production of IL-1β, TNF-α and IL-6 pro-inflammatory cytokines and the proliferation of immune cells in the presence of specific stimuli for macrophages, B-lymphocytes and T-lymphocytes were evaluated after treatment with both GOs.

3.1. Characterization of GO nanosheets

As it was confirmed by Transmission Electron Microscopy (TEM) and Dynamic Light Scattering (DLS) in our previous works, the chemical exfoliation of graphite resulted on thin nanosheets of 3–4 layers of graphene oxide, with average thickness of 1.8 nm and size distribution within the range approximately 10–120 nm with the maximum number of particles located around 40 nm [33,34]. As it can be observed in Fig. 1, XPS analysis of the GO nanosheets showed high oxygen contents on its structure, with a C/O ratio of 1.8, that corresponds essentially to the following oxygen functional groups C—O—C/C—OH (287.2 eV) and C=O/COOH (288.7 eV). An evaluation of the GO nanosheets structure has been performed by analyzing the D and G bands typical of carbon struc-

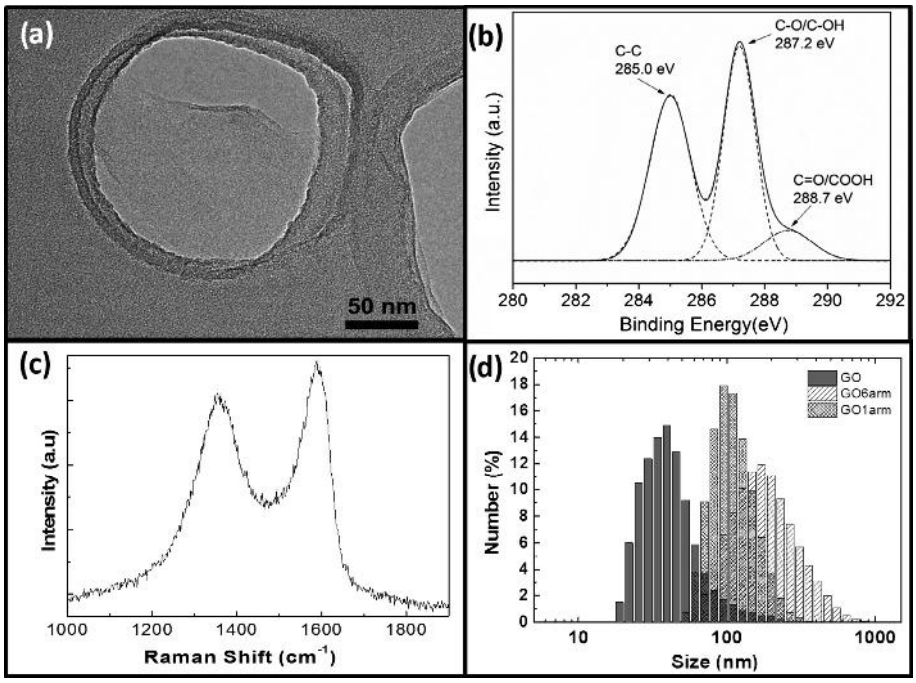

Fig. 1. (a) Transmission electron micrograph of GOs, (b) high-resolution C1s spectra of the graphene oxide nanosheets, (c) Raman spectrum of GOs, and (d) GOs particle size distribution obtained by DLS analysis.

tures of the Raman spectra (Fig. 1c). Raman spectra showed a typical shape of 488 nm excitation wavelength.

Graphene oxide surfaces subjected to successful pegylation procedure were monitored by FTIR spectra and resulted in the presence of the oxygen functionalities at GO surface plus the C—O stretch vibration band (110–150 cm^{-1}) and the strong C—H stretch peak (2800 cm^{-1}) demonstrating the presence of the PEG on the GO sample (data not shown).

Both GOs with 1 (1-GOs) and 6 arms (6-GOs) of PEG were also characterized by amine quantification and by the zeta potential measurements [34]. High branched PEG is commonly used for functionalizing nanoparticles intended for nanomedicine, more specifically 6-arm PEG is used because of being a versatile platform for the attachment of different molecules due to the high amount of branches available for performing the chemistry. Nevertheless, as we published previously, the size of the molecule is large and increases the overall hydrodynamic size of the nanosystem (PEG-GO) having negative effects when interacting with the cells. The linear version of the PEG, is smaller and has the same non-fouling properties, while producing less toxicity and higher nanoparticle uptake when compared to the high branched version. However, as high branched polymers are still widely used, it is important to study the possible and potential side effects of both in order to be able in a future of choosing the more suitable one for this application. As it can be seen in Fig. 1d, particle sizes increases reaching a distribution maximum of 100 nm for 1-arm PEGylated GO nanosheets and showing a wider distribution of sizes with a maximum of approx 300 nm for 6-arm PEGylated GO nanosheets.

3.2. In vitro effects of GO nanosheets on RAW-264.7 macrophages

Since these PEG-GO nanosheets (1-GOs and 6-GOs) were designed for hyperthermia cancer therapy, different cell types were chosen in previous studies in order to evaluate the GOs uptake by human osteosarcoma cell line Saos-2 and to know how the cells surrounding the tumor could be affected by the incorporation of these materials. Thus, Saos-2 osteoblasts, MC3T3-E1 preosteoblasts, L929 fibroblasts and RAW-264.7 macrophages were used as *in vitro* experimental models, measuring the incorporation of both 1-GOs and 6-GOs (labelled with FITC) by each cell type and evaluating the effects of this uptake on cell proliferation, viability and intracellular ROS content [33,34]. Previous results demonstrated that these different cell types can proliferate *in vitro* in contact with either 1-GOs or 6-GOs which induced significant growth delays. RAW-264.7 macrophages were the cell type more affected by GOs when it was compared with Saos-2 osteoblasts, MC3T3-E1 preosteoblasts and L929 fibroblasts [34]. However, when the FITC-GO incorporation was evaluated by flow cytometry, the uptake of both 1-GOs and 6-GOs by RAW macrophages was lower than the incorporation by the other three cell types. The effects of 1-GOs and 6-GOs on the proliferation of RAW-264.7 macrophages were accompanied by some cell cycle alterations which can be connected with apoptosis [35,36] through increased production of reactive oxygen species (ROS) and intracellular Ca^{2+} levels as well as by decreased mitochondrial membrane potential [36,37].

Since RAW-264.7 cells retain many of the characteristics of macrophages *in vivo* [38], in the present study RAW cells were cultured with 1-GOs and 6-GOs to evaluate the production of IL-1β, TNF-α and IL-6 as pro-inflammatory cytokines after GOs uptake. Figs. 2 and 3 show the incorporation of 1-GOs and 6-GOs labelled with FITC by RAW-264.7 macrophages after 1 day treatment evaluated by confocal microscopy. 1-GOs uptake was higher than 6-GOs incorporation in agreement with previous results [33,34]. Typical macrophage morphology and high values of cell viability, evaluated by propidium iodide exclusion (over 80–90%, data not shown) were obtained. When cells were stained with DAPI for the visualization of the cell nuclei in blue (Figs. 2A and 3A) and with rhodamine-phalloidin for cytoplasmic F-actin filaments in red (Figs. 2B and 3B), the confocal images showed that both 1-GOs and 6-GOs labelled with FITC (green) (Figs. 2C and 3C) colocalize with rhodamine-phalloidin (red) resulting in yellow/orange coloration (Figs. 2D and 3D), as it was previously observed [33]. The fluorescence intensity in the images of cells treated with

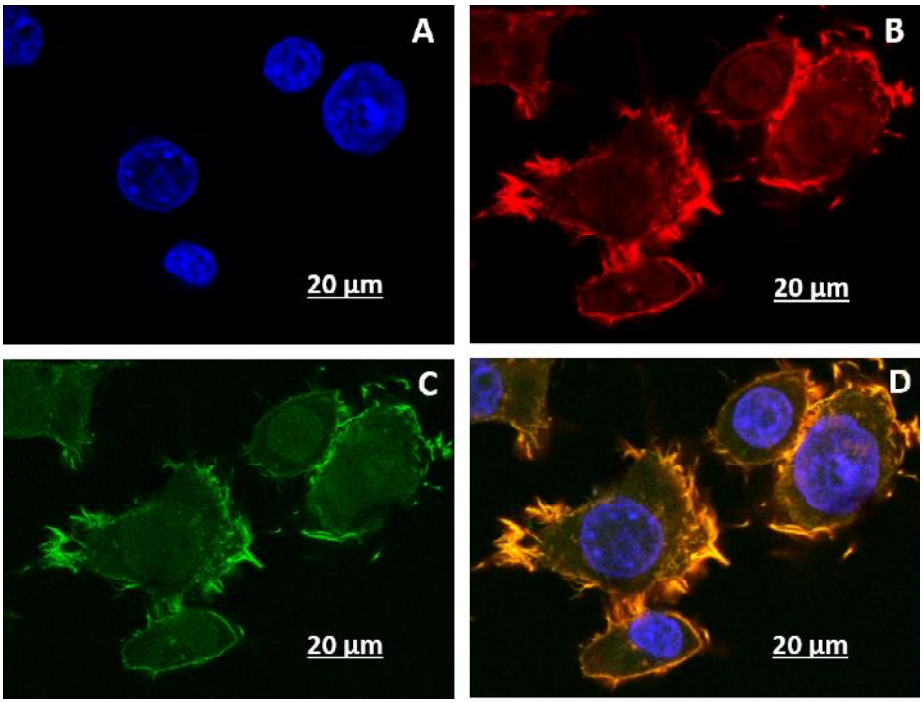

Fig. 2. Morphology evaluation by confocal microscopy of murine RAW-264.7 macrophages after 1 day treatment with 1-GOs. Cells were stained with DAPI for the visualization of the cell nuclei in blue (A), rhodamine-phalloidin for cytoplasmic F-actin filaments in red (B) and FITC-GOs in green (C). Overlay of the three stainings (D) reveals that FITC-GOs colocalizes with rhodamine-phalloidin resulting in yellow/orange coloration. (For interpretation of the references to colour in this figure legend, the reader is referred to the web version of this article.)

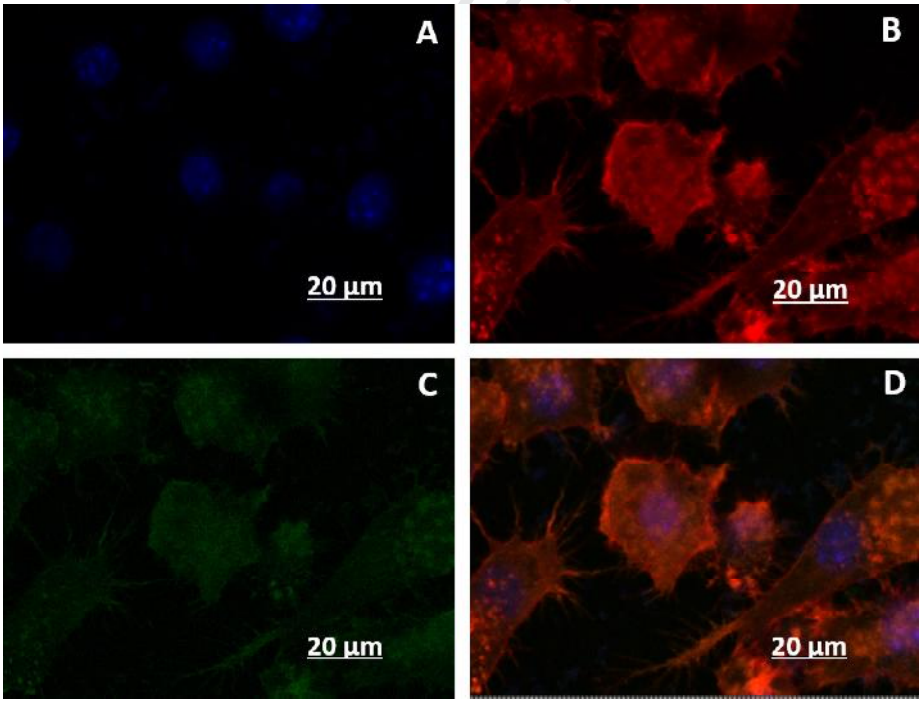

Fig. 3. Morphology evaluation by confocal microscopy of murine RAW-264.7 macrophages after 1 day treatment with 6-GOs. Cells were stained with DAPI for the visualization of the cell nuclei in blue (A), rhodamine-phalloidin for cytoplasmic F-actin filaments in red (B) and FITC-GOs in green (C). Overlay of the three stainings (D) reveals that FITC-GOs colocalizes with rhodamine-phalloidin resulting in yellow/orange coloration. (For interpretation of the references to colour in this figure legend, the reader is referred to the web version of this article.)

1-GOs (Fig. 2) was higher than with 6-GO (Fig. 3), in agreement with flow cytometry analysis (data not shown). Recent studies demonstrate that when naive macrophages are incubated with conditioned medium collected from graphene-exposed macrophages, the actin assembly and the expansion of podosomes are affected, adhesion of macrophages to the extracellular matrix is decreased, and phagocytosis is attenuated [37]. It is known that the cellular uptake of nanoparticles is cell-line dependent as

particle binding depends on cell surface properties which are critical for these interactions [39,40]. Some authors have recently evaluated a series of cellular responses including the cellular uptake of GO sheets with different size and using different cell types [41]. In terms of capacity to internalize GOs, some differences were observed between non-phagocytic cells and macrophages. Thus, the capacity of internalizing 350 nm and 2 μm GO sheets was higher in macrophages [20]. However, it has also been reported that escape from the phagocytic uptake is induced by maintaining the particle size around 150 nm. In addition, particles of small sizes might exhibit a high level of exocytosis [42,43]. On the other hand, endocytic pathways involved in particle uptake have been investigated in nonphagocytic cells [42,43] showing that they use more than one pathway to internalize particles, but it is assumed that particles up to 200 nm are internalized mainly by receptor-mediated endocytosis. Recent studies demonstrate that graphene quantum dots are internalized primarily through caveolae-mediated endocytosis and their cytotoxicity is lower than that of the micrometer-sized GO [44]. It has been already reported [33] for polymeric nanoparticles that fibroblasts have one of the lowest nanoparticle uptake rates. Concerning the higher incorporation of 1-GOs in comparison to 6-GOs observed with different cell types [33,34], it could be explained because of the different sizes of these sheets. Thus, 6-GOs nanoparticles, with larger sizes than 1-GOs, need a stronger driving force and additional energy in the cellular internalization process [33,45].

Macrophages can synthesize and release a large variety of cytokines upon stimulation by exogenous or endogenous factors. These cytokines can modulate most macrophage functions and the expression of cell surface markers [46]. To investigate the influence of GOs exposure on the secretion of cytokines by macrophages, IL-1β, TNF-α, and IL-6 content in the supernatants of murine RAW-264.7 cells which were incubated overnight either in the absence or in the presence of 1 μg/ml lipopolysaccharide (LPS *E. coli* 055:B5) and then with 75 μg/ml of either 1-GOs or 6-GOs during 1 day. LPS was used to induce the inflammatory response. The GO doses used in the present study are within the optimal range of previous studies which have shown good results concerning the incorporation in RAW-264.7 macrophages as well as an effective induction of cell death *in vitro* after irradiating tumoral osteoblasts with internalized 1-GOs [47].

As shown in Fig. 4, only the exposure of RAW-264.7 macrophages stimulated with lipopolysaccharide (LPS) to 6-GOs significantly increased the secretion of TNF-α when compared to other conditions. The secretion of IL-6 and IL-1β cytokines was not modified in these experimental conditions (data not shown). Previous studies with Saos-2 osteoblasts demonstrated that both materials induced a significant decrease of IL-6 levels, more pronounced after 72 h treatment with 6-GOs [36].

Anderson et al. found that macrophages on a biomaterial surface that does not promote fusion secrete higher levels of the pro-inflammatory cytokines IL-1β and IL-6. On the other hand, TNF-α is known to be responsible for apoptosis of biomaterial-adherent macrophages [48]. Since macrophage is a primary immune cell type resident in tissues, recent data suggest that *in vivo* administration of GO at high concentration may elicit induction of TNF-α, IFN-γ, and IL-2 that can modulate ensuing adaptive immune responses. Recently, other authors have studied the impact of functionalized carbon nanotubes (f-CNT) and graphene on immune cells showing that some f-CNTs can directly elicitate specific inflammatory pathways [49]. Thus, these findings underscore the importance of further scrutinizing safe application of GO *in vivo* [50–52].

3.3. In vitro effects of GO nanosheets on primary splenocytes

In the present study, the *in vitro* evaluation of the 1-GOs and 6-GOs effects on different immune cell types involved in the immune response have been also performed using murine primary spleno-

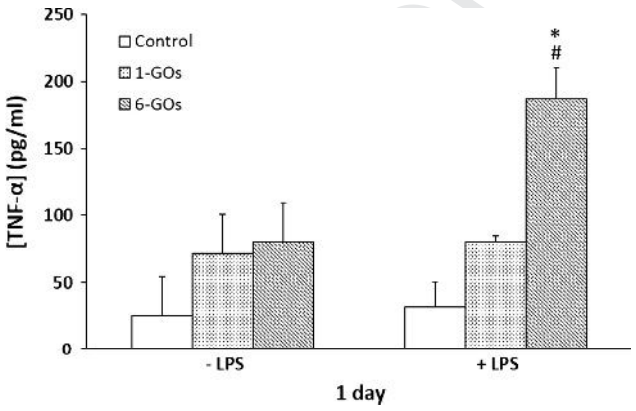

Fig. 4. Effects of 1-GOs and 6-GOs on TNF-α release by murine RAW-264.7 macrophages after 1 day treatment. Cells were incubated overnight either in the absence or in the presence of 1 μg/ml LPS (*E. coli* 055:B5) and then with GO materials (75 μg/ml) during 1 day. Controls without GOs were carried out in parallel. Statistical significance: $^{*}p < 0.05$ (compared to control without material) and $^{\#}p < 0.05$ (compared to sample without LPS).

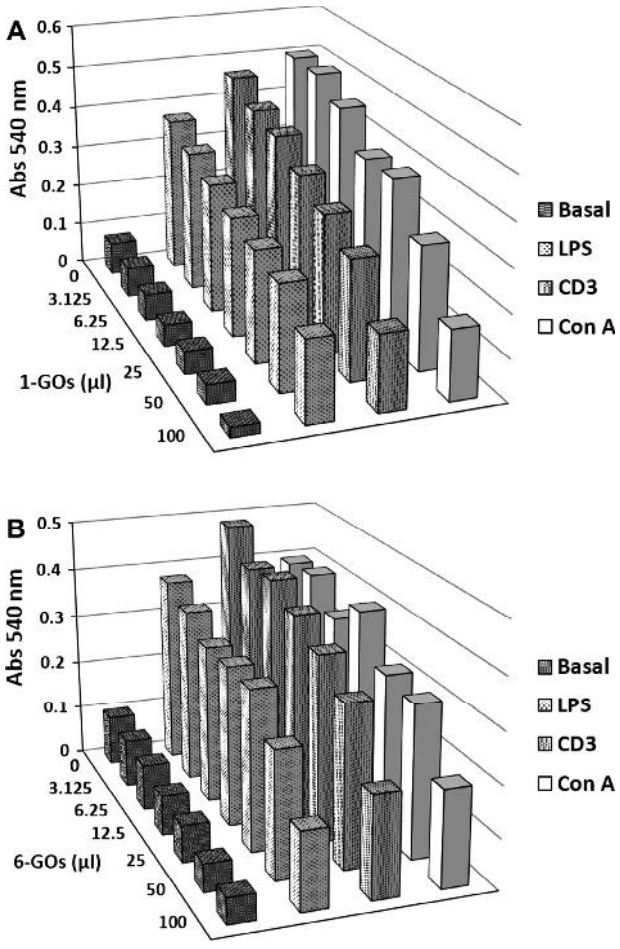

Fig. 5. Effects of *in vitro* exposure to 1-GOs and 6-GOs of spleen cells. Proliferative response in the presence of different concentrations (75 μg/ml, 100, 50, 25, 12.5, 6.25, 3.125 μl/well) of 1-GOs (A) and 6-GOs (B) of primary murine splenocytes unstimulated or stimulated by soluble antibody to CD3 (YCD3-1) (5 μg/ml), LPS (100 μg/ml), or Con A (2.5 μg/ml).

Please cite this article in press as: M.J. Feito et al., J. Colloid Interface Sci. (2014), http://dx.doi.org/10.1016/j.jcis.2014.07.004

cytes. This experimental model represents an approximation to the *in vivo* situation because primary spleen cells are cultured in contact with GOs and different untransformed normal cell subpopulations interact in among them, better approaching the *in vivo* ambient. As one of the primary lymphoid tissues, the spleen filters peripheral blood and consists primarily of B-cells and T-cells (lymphocytes), as well as macrophages and *natural killer* cells. Spleens from C57BL/6 mice were aseptically obtained and then, single-cell suspensions were prepared and cultured for 24 h with different doses of either 1-GOs or 6-GOs. Modulation of cell-mediated responses was assessed by evaluating T-cell proliferation (induced by either anti-CD3 antibody or concanavalin A) and B-cell/macrophage proliferation (induced by lipopolysaccharide, LPS). Since primary immune cells are more sensitive than RAW-264.7 macrophages, different lower doses of both GOs were assayed with primary murine splenocytes to avoid cell damage. Proliferation data for these immune cell sub-populations are summarized in Figs. 5 and 6.

Only a basal proliferation level of less than 0.1 O.D. was detected in cultures with 1-GOs and 6-GOs without stimulus. On the other hand, no significant differences were obtained among the basal levels with the six GOs concentrations used in this study. Specific stimuli of either T lymphocytes (ConA, anti-CD3) or B lymphocytes/macrophages (LPS) induced a vigorous activation and cell proliferation (Fig. 5A and B). The addition of different doses of 1-GOs and 6-GOs significantly reduced the proliferation of all these immune cell sub-populations in the presence of each stimulus in a dose-dependent manner, as it can be observed in Fig. 6A and B. When the effect of 1-GOs and 6-GOs is compared, a more pronounced proliferation decrease is observed after treatment with 1-GOs in the presence of the different stimuli, in agreement with the higher incorporation of this material (Fig. 2). However, the statistical analysis of these data shows that these differences between the effect of 1-GOs and 6-GOs are not significant (Fig. 6A and B).

To obtain more data on proinflammatory response of murine splenocytes to GOs, supernatants from the proliferation experiments were analyzed to quantify IL-6, IL-1β and TNF-α levels. As it can be observed in Fig. 7A and B, the production of IL-6 is significantly increased in the presence of LPS (which stimulates B-cells and macrophages), in comparison with the basal situation without stimulus. Interestingly, a high dose of 1-GOs (Fig. 7A) or 6-GOs (Fig. 7B) decreased this LPS effect. The addition of anti-CD3 or concanavalin A (that primarily stimulate T lymphocytes) also produces significant increase of this cytokine in the absence of material (Fig. 7A and B). When splenocytes are treated with 1-GOs in the presence of anti-CD3 or concanavalin A, the IL-6 secretion decreases in a dose-dependent manner and the values are not significantly different of the basal situation (Fig. 7A). However, the treatment with 6-GOs do not decrease the IL-6 values except in the presence of anti-CD3 (Fig. 7B). These results evidence that 6-GOs produces a lower effect than 1-GOs on T cells (stimulated specifically by concanavalin A and anti-CD3). A decrease of IL-6 secretion produced by GOs has been previously obtained when Saos-2 osteoblast were cultured with both GOs [34]. Recent results indicate that the secretion of proinflammatory cytokines is strongly dependent on the GO dosage, incubation time and

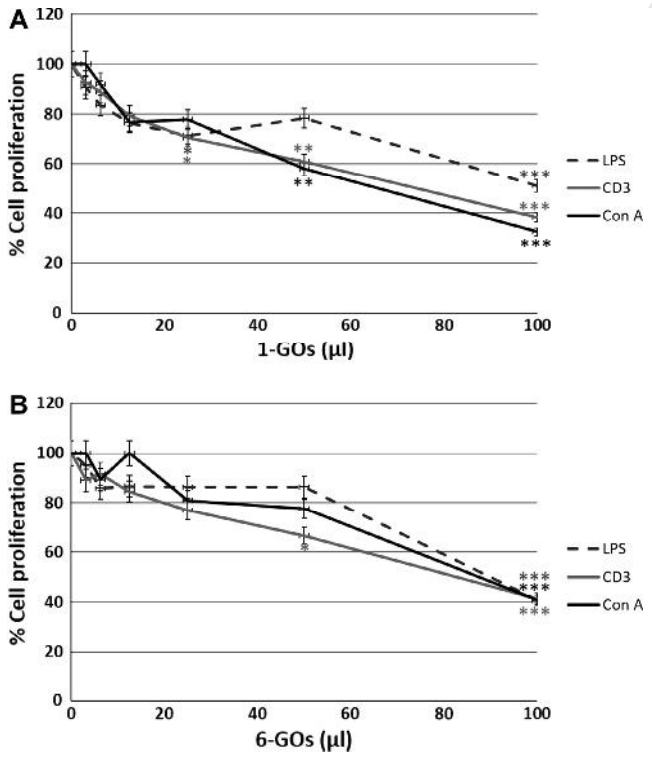

Fig. 6. Effects of *in vitro* exposure to 1-GOs and 6-GOs of spleen cells. Cell percentage of spleen cells in the presence of different concentrations (75 μg/ml, 100, 50, 25, 12.5, 6.25, 3.125 μl/well) of 1-GOs (A) and 6-GOs (B) of primary murine splenocytes unstimulated or stimulated by soluble antibody to CD3 (YCD3–1) (5 μg/ml), LPS (100 μg/ml), or Con A (2.5 μg/ml). The proliferation is shown as percentage in relation to controls (100%) in the absence of material, as determined by a colorimetric MTT assay. $^{*}p < 0.05$, $^{**}p < 0.01$, $^{***}p < 0.005$.

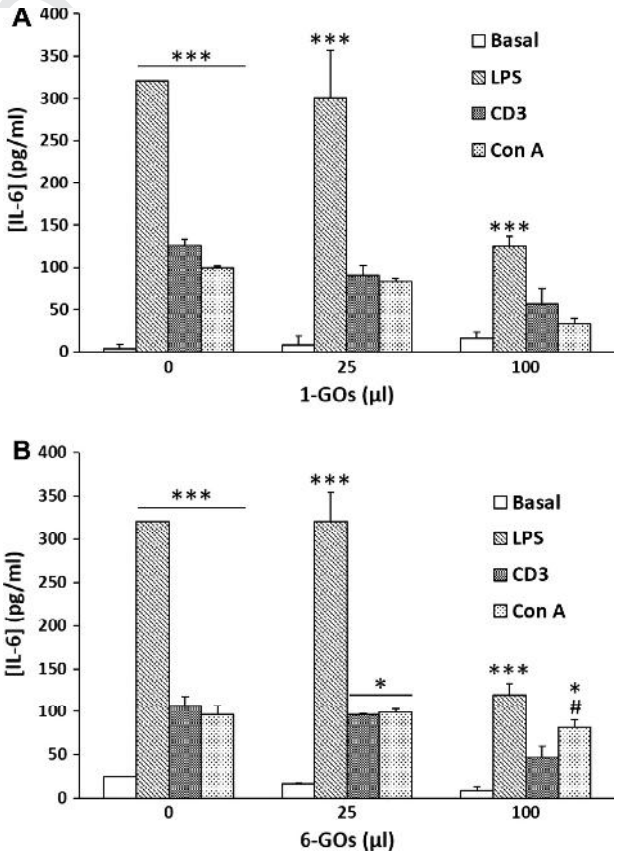

Fig. 7. Effects of 1-GOs (A) and 6-GOs (B) on IL-6 release by primary murine splenocytes. Cells were activated for 24 h with anti-CD3 (YCD3–1) (5 μg/ml), LPS (100 μg/ml), or Con A (2.5 μg/ml), in the presence or absence of GOs at 75 μg/ml (25, 100 μl/well), as indicated. IL-6 was determined in the supernatants by capture ELISA as described in Section 2. Controls without material were also carried out. The results obtained are expressed as concentration (pg/ml) and were compared with basal values to obtain their statistical significance. $^{*}p < 0.05$, $^{***}p < 0.005$ (compared to basal values) and $^{\#}p < 0.05$ (compared between 1-GOs and 6-GOs).

particularly on the GO micro-size [20]. Thus, IL-6, IL-12, TNF-α, MCP-1, and IFN-γ, were significantly increased after 48 h in the medium of cells treated with 2 nm GO nanosheets. However, a weak increase of these mediators was observed using 350 nm GOs.

No significant changes were detected when IL-1β and TNF-α levels were quantified after treatment of primary splenocytes with both 1-GOs and 6-GOs in the experimental conditions of the present study (data not shown).

These data indicate clear differences between spleen cells and RAW macrophages concerning the effect of GOs on inflammatory cytokine secretion that needs to be analyzed in future studies using purified immune cell populations.

4. Conclusions

Previous results demonstrated that graphene oxide nanosheets (GOs) with 1 and 6 arms of polyethylene glycol, designed for hyperthermia cancer therapy, induced significant growth delays in different cell types [33,34]. The evaluation of the effects of both GOs on the macrophage activity and on the B- and T-lymphocyte responses induced by specific stimuli, indicates in the present study that these materials reduce immune cell proliferation and do not stimulate proinflammatory cytokine secretion. These weak inflammation properties can be favourable for hyperthermia cancer therapy with these GOs.

Acknowledgments

This study was supported by research grants from Spanish CICYT (Project MAT2008-00736), CAM (Project S2009/MAT-1472) and Ministerio de Ciencia e Innovación (Project CSO2010-11384-E). J.M. Rojo is supported by Grant PI10/00650 from "Plan Estatal I+D+i", ISCIII-Subdirección General de Evaluación y Fomento de la Investigación, Ministerio de Economía y Competitividad (MINECO), Spain. M.C. Matesanz and J. Linares are greatly indebted to MICINN and CIBER-BBN respectively for predoctoral fellowships. M. Vila thanks the Spanish Ministry for the RyC grant and the Fundação para a Ciência e Tecnologia (FCT) Investigator Program 2012. Gil Gonçalves thanks the Fundação para a Ciência e Tecnologia (FCT) for the PostDoc grant (SFRH/BDP/84419/2012). P. Marques thanks FCT for the Investigator Program 2013. TEMA research unit also thanks FCT for TEMA (PEst-C/EME/UI0481/2013). The authors wish to thank also to the staff of the Cytometry and Fluorescence Microscopy Center of the Universidad Complutense de Madrid (Spain) for the assistance in the flow cytometry and confocal microscopy studies.

References

[1] R. Ruoff, Nat. Nanotechnol. 3 (2008) 10–11.
[2] X. Sun, Z. Liu, K. Welsher, J.T. Robinson, A. Goodwin, S. Zaric, H. Dai, Nano Res. 1 (2008) 203–212.
[3] L. Zhang, J. Xia, Q. Zhao, L. Liu, Z. Zhang, Small 6 (2010) 537–544.
[4] H. Fan, L. Wang, K. Zhao, N. Li, Z. Shi, Z. Ge, Z. Jin, Biomacromolecules 11 (2010) 2345–2351.
[5] D. Depan, B. Girase, J.S. Shah, R.D. Misra, Acta Biomater. 7 (2011) 3432–3445.
[6] K. Yang, S. Zhang, G. Zhang, X. Sun, S.T. Lee, Z. Liu, Nano Lett. 10 (2010) 3318–3323.
[7] N.W. Kam, M. O'Connell, J.A. Wisdom, H. Dai, Proc. Natl. Acad. Sci. USA 102 (2005) 11600–11605.
[8] X.Y. Yang, Y.S. Wang, X. Huang, Y.F. Ma, Y. Huang, R.C. Yang, H. Duan, J. Mater. Chem. 21 (2011) 3448–3454.
[9] S.R. Ryoo, Y.K. Kim, M.H. Kim, D.H. Min, ACS Nano 4 (2010) 6587–6598.
[10] V.C. Sanchez, A. Jachak, R.H. Hurt, A.B. Kane, Chem. Res. Toxicol. 25 (2012) 15–34.
[11] L. Feng, Z. Liu, Nanomedicine 6 (2011) 317–324.
[12] G. Gonçalves, M. Vila, M.T. Portolés, M. Vallet-Regi, J. Gracio, P.A. Marques, Adv. Healthc. Mater. 2 (2013) 1072–1090.
[13] G. Storm, S.O. Belliot, T. Daemen, D. Lasic, Adv. Drug Deliv. Rev. 17 (1) (1995) 31–48.
[14] Z. Liu, J.T. Robinson, X. Sun, H. Dai, J. Am. Chem. Soc. 130 (2008) 10876–10877.
[15] Y. Chang, S.T. Yang, J.H. Liu, E. Dong, Y. Wang, A. Cao, Y. Liu, H. Wang, Toxicol. Lett. 200 (2011) 201–210.
[16] K. Wang, J. Ruan, H. Song, J. Zhang, Y. Wo, S. Guo, D. Cui, Nanoscale Res. Lett. 6 (2011) 8.
[17] L. Horváth, A. Magrez, M. Burghard, K. Kern, L. Forró, B. Schwaller, Carbon 64 (2013) 45–60.
[18] M.J. Smith, K.L. White Jr., D.C. Smith, G.L. Bowlin, Biomaterials 30 (2009) 149–159.
[19] M. Alcaide, P. Portolés, A. López-Noriega, D. Arcos, M. Vallet-Regí, M.T. Portolés, Acta Biomater. 6 (2010) 892–899.
[20] H. Yue, W. Wei, Z. Yue, B. Wang, N. Luo, Y. Gao, D. Ma, G. Ma, Z. Su, Biomaterials 33 (2012) 4013–4021.
[21] R. Medzhitov, C.A. Janeway Jr., N. Engl. J. Med. 343 (2000) 338–344.
[22] S. Franz, S. Rammel, D. Scharnweber, J.C. Simon, Biomaterials 32 (2011) 6692–6709.
[23] D.T. Chang, E. Colton, J.M. Anderson, J. Biomed. Mater. Res. A 89 (2009) 490–498.
[24] M.A. Duque Correa, M. Rojas López, Inmunología 26 (2007) 73–86.
[25] A. Katrin, J. Barth, D. Waterfield, D.M. Brunette, J. Biomed. Mater. Res. A 101 (2013) 2679–2688.
[26] S.M. van Putten, D.T.A. Ploeger, E.R. Popa, R.A. Bank, Acta Biomater. 9 (2013) 6502–6510.
[27] W.G. Brodbeck, M. MacEwan, E. Colton, H. Meyerson, J.M. Anderson, J. Biomed. Mater. Res. A 74 (2005) 222–229.
[28] A. Rodriguez, M. James, J. Biomed. Mater. Res. A 92 (2010) 214–220.
[29] A. Schinwald, F.A. Murphy, A. Jones, W. MacNee, K. Donaldson, ACS Nano 6 (2012) 736–774.
[30] G. Gonçalves, P.A. Marques, C. Granadeiro, H.I.S. Nogueira, M.K. Singh, J. Grácio, Chem. Mater. 21 (2009) 4796–4802.
[31] P. Portoles, J.M. Rojo, A. Golby, M. Bonneville, S. Gromkowski, L. Greenbaum, C.A. Janeway Jr., D.B. Murphy, K. Bottomly, J. Immunol. 142 (1989) 4169–4175.
[32] T. Mosmann, J. Immunol. Methods 65 (1983) 55–63.
[33] C. Matesanz, M. Vila, M.J. Feito, J. Linares, G. Gonçalves, M. Vallet-Regi, P.A. Marques, M.T. Portolés, Biomaterials 34 (2013) 1562–1569.
[34] M. Vila, M.T. Portolés, P.A. Marques, M.J. Feito, M.C. Matesanz, C. Ramírez-Santillán, G. Gonçalves, S.M. Cruz, A. Nieto, M. Vallet-Regi, Nanotechnology 23 (2012) 465103. 9.
[35] B. Sun, S. Geng, X. Huang, J. Zhu, S. Liu, Y. Zhang, J. Ye, Y. Li, J. Wang, Cancer Lett. 301 (2011) 95–105.
[36] C.S. Yu, A.C. Huang, J.S. Yang, C.C. Yu, C.C. Lin, H.K. Chung, I.P. Huang, F.S. Chueh, J.G. Chung, Anticancer Res. 32 (2012) 1671–1679.
[37] Y. Li, Y. Liu, Y. Fu, T. Wei, L.L. Guyader, G. Gao, R.S. Liu, Y.Z. Chang, C. Chen, Biomaterials 33 (2012) 402–411.
[38] W.C. Raschke, S. Baird, P. Ralph, I. Nakoinz, Cell 15 (1978) 261–267.
[39] S. Yu, C.M. Lau, S.N. Thomas, W.G. Jerome, D.J. Maron, J.H. Dickerson, J.A. Hubbell, Int. J. Nanomed. 7 (2012) 799–813.
[40] C. He, Y. Hu, L. Yin, C. Tang, C. Yin, Biomaterials 31 (2010) 3657–3666.
[41] C. Cortez, E. Tomaskovic-Crook, A.P.R. Johnston, A.M. Scott, E.C. Nice, J.K. Heath, F. Caruso, ACS Nano 1 (2007) 93–102.
[42] I. Slowing, B.G. Trewyn, B.S.Y. Lin, J. Am. Chem. Soc. 128 (2006) 14792–14793.
[43] W. Busch, S. Bastian, U. Trahorsch, M. Iwe, D. Kühnel, T. Meißner, A. Springer, M. Gelinsky, V. Richter, C. Ikonomidou, A. Potthoff, I. Lehmann, K. Schirmer, J. Nanopart. Res. 13 (2010) 293–310.
[44] C. Wu, C. Wang, T. Han, X. Zhou, S. Guo, J. Zhang, Adv. Healthc. Mater. 2 (2013) 1613–1619.
[45] Z.G. Yue, W. Wei, P.P. Lv, H. Yue, L.Y. Wang, Z.G. Su, G.H. Ma, Biomacromolecules 12 (2011) 2440–2446.
[46] H. Zhou, K. Zhao, W. Li, N. Yang, Y. Liu, C. Chen, T. Wei, Biomaterials 33 (2012) 6933–6942.
[47] M. Vila, M.C. Matesanz, G. Gonçalves, J. Feito M, J. Linares, P.A. Marques, M.T. Portolés, M. Vallet-Regí, Nanotechnology 25 (2014). 035101.
[48] J.M. Anderson, A. Rodriguez, D.T. Chang, Semin. Immunol. 20 (2008) 86–100.
[49] M. Orecchioni, D. Bedognetti, F. Sgarrella, F. Marincola, A. Bianco, L.G. Delogu, J. Transl. Med. 12 (2014) 138.
[50] GY1 Chen, H.J. Yang, C.H. Lu, Y.C. Chao, S.M. Hwang, C.L. Chen, K.W. Lo, L.Y. Sung, W.Y. Luo, H.Y. Tuan, Y.C. Hu, Biomaterials 33 (2012) 6559–6569.
[51] K. Kostarelos, K.S. Novoselov, Science 344 (2014) 261–263.
[52] A. Bianco, Angew. Chem. Int. Ed. Engl. 52 (2013) 4986–4997.